

# 2

## Planetary environments

The primary goal for a planetary rover is to navigate and traverse an unknown, hostile terrain, recognize and negotiate obstacles, deploy scientific instrumentation, and acquire samples from scientific targets. The range of planetary environments is vast ranging from the relatively benign and flat to extremely rocky and hostile. Most terrestrial mobile robotics platforms are operated in relatively benign environments such as office corridors and the like despite recent emphasis on “embodied” or “situated” robotics paradigms which emphasize the necessity for dealing with realistic (and so uncompromising) environments [37, 38]. Terrestrial mobile robotics research tends to employ primitive mobility systems such as differential drives and tricycle configurations involving two powered wheels and a castor wheel [39]. Planetary robotics does not have that luxury—planetary environments are rugged, hostile, and a priori unknown (e.g., the Martian terrain is both rocky and sandy, Figure 2.1). Planetary rovers have a number of additional critical constraints that are generally absent from traditional terrestrial mobile robots [40]:

- (i) adverse terrain characterized by rocks, cliffs, crevasses, etc. with few features for self-localization;
- (ii) lack of a priori data on specific features of this environment to be explored;
- (iii) extensive signal time-of-flight and limited communication windows to Earth implying a need for high degrees of autonomy;
- (iv) hostile ambient conditions including thermal extremes and dust environments;
- (v) limited power availability;
- (vi) high-reliability requirements which limit mechanical complexity.

It is these issues, which impose more stringent constraints on planetary rovers than are normally traditionally associated with terrestrial mobile robots, that have significant impact on the design and methodologies employed in planetary rovers. The chassis typically comprises around 30% of the rover’s total mass.

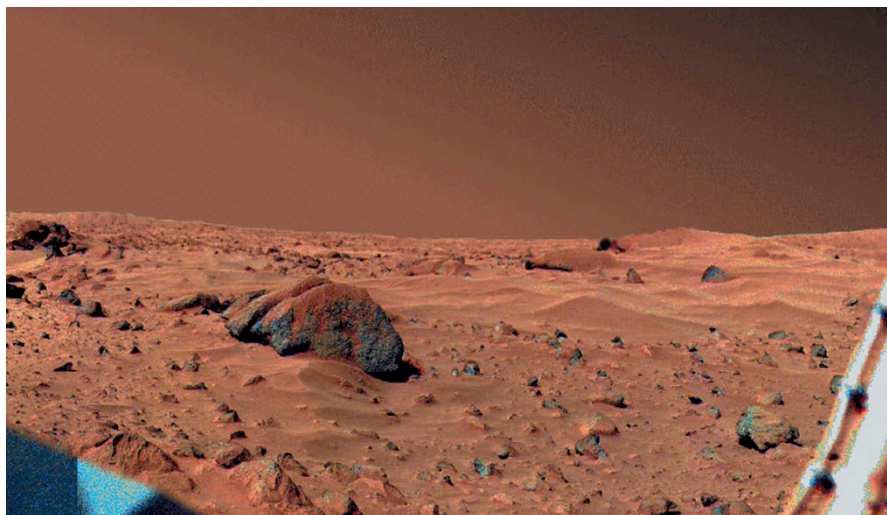
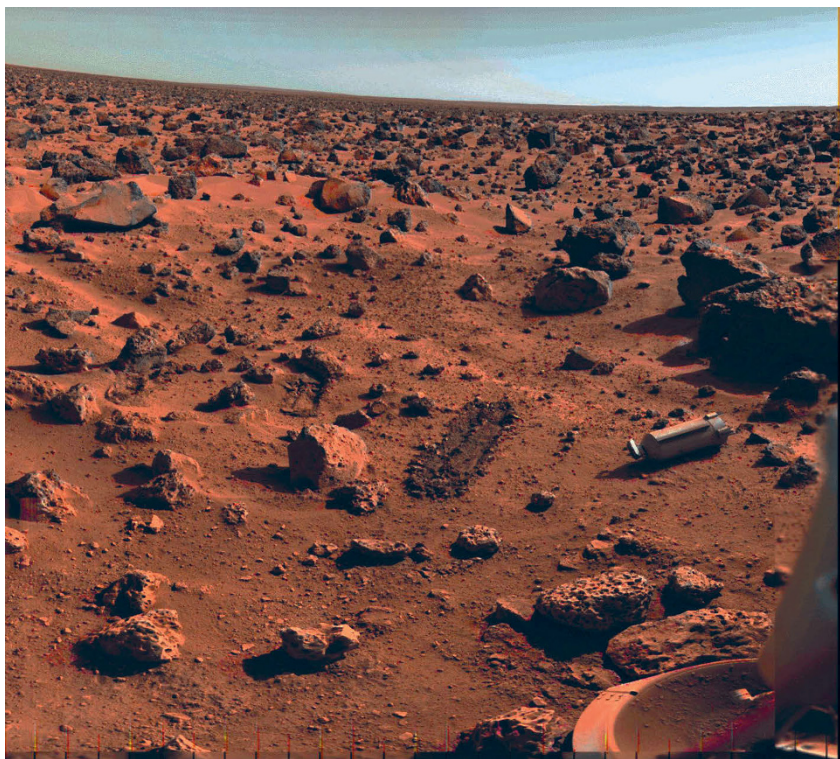


**Figure 2.1.** Terrain on Mars: (a) rocky and (b) sandy [credit NASA JPL].

The NATO Reference Mobility Model (NRMM) emphasizes performance characteristics based on [41]: (i) maximum speed and turning radius; (ii) traction for overcoming resistive forces to motion; (iii) vehicle maneuverability for obstacle avoidance; (iv) ride comfort. Performance parameter (iv) is not considered further as suspension is not generally regarded as high priority for robotic rovers and traversal speeds of planetary rovers are low  $\sim 10\text{--}20\text{ cm/s}$ —low speeds under  $3\text{ m/s}$  imply that quasistatic analysis is sufficient to characterize their dynamics. Performance parameter (i) is determined by parameters (ii) and (iii). Maximum speed will be determined by: (i) motor torques; (ii) slopes; (iii) incidence of obstacles (which determines mean free path); (iv) surface traction on soil. Turning radius will depend on the geometry of the vehicle and the nature of the turning mode and strongly influences parameter (iii)—skid steering which is adopted in tracked vehicles and small microrover vehicles offers the highest turning maneuverability at the expense of power consumption. Most vehicles with forward and aft motion capability can turn through skid steering. Ackermann steering is commonly implemented on planetary rovers at or above the microrover class.

All terrestrial surfaces are covered in fragmented grains resultant from  $\sim$ physical fracturing of surface rock by impact flux, thermal cycling, and chemical or other types of weathering—regolith which is similar in constitution to terrestrial soil but without soil's moisture and organic constituents. Lunar soil is more finely fragmented with fewer boulders than Mars due to the lack of an atmosphere to filter out micrometeorite bombardment. We consider the most popular venues for rover missions—the Moon and Mars—but rover missions are not exclusive to these planets (e.g., Venus, gas giant moons, small bodies of the Solar System, etc.). There are certain features common to most terrestrial planets, the Moon and Mars especially. The properties of the lunar regolith are known from both in situ measurements and returned samples. The properties of Martian soil are known to a much lesser degree through in situ measurements. In general, extraterrestrial environments are characteristically dry which has implications for the physical properties of the regolith. This is not the case for gas giant moons of interest—Europa (Figure 2.2), Ganymede, Callisto, and Enceladus—which are essentially covered in icy surfaces with evidence of liquid water flows.

The nature of planetary terrain will have the greatest influence on the selection of the rover chassis design which in turn imposes implications for rover mass and power design budgets. For this reason, planetary rover design begins with a reference terrain. Similarly, like all spacecraft that have landed on planetary surfaces, rovers are designed for hostile environmental conditions that are rare or absent on Earth. The planetary day/night cycle imposes thermal cycling and deep thermal loads: for instance, a Martian day (sol) is slightly longer than Earth's and Mars is farther from the Sun than Earth but the ambient temperature is mediated by the Martian atmosphere; the Moon has a 2-week day/2-week night and resides at essentially the same distance from the Sun as Earth but there is direct exposure to the Sun or the cold of deep space. The distance to the Earth impacts the rover communications architecture limiting teleoperation to the Moon and necessitating

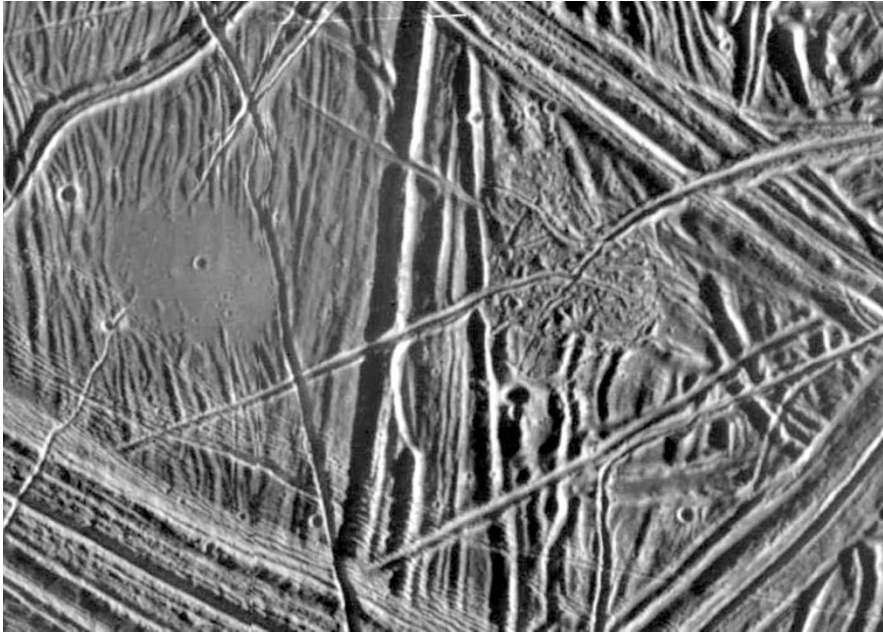


**Figure 2.2.** Surface of Europa [credit NASA JPL].

autonomous behavior for Mars operations. General spacecraft design issues relevant to planetary rover design are covered in other texts [42].

## 2.1 THE MOON

The Moon is a high priority for robotic exploration prior to human missions [43]. Although U.S. intentions towards the Moon are unclear at present, China's ambitions are focused on the Moon. This began with its first manned launch in 2003, followed by robotic missions—Chang'e-1 and Chang'e-2 orbiters and Chang'e-3 the lander/rover—to the Moon. These are due to be followed by the Chang'e-4 carrying another lander and rover to the lunar surface, and finally Chang'e-5 to return samples from the Moon. China is also committed to its manned space station laboratory Tiangong-1. The Moon has a surface gravity of  $1.62\text{ m/s}^2$  and a temperature variation of 120–380 K at the equator and as low as 40 K at the poles. It has no atmosphere. Its crust has an average thickness of 70 km being thinner on the nearside than on the farside. Below the crust is its mantle which overlies a small solid core of  $\sim 340\text{ km}$  radius. The Moon therefore has no global magnetic field but some of its surface rocks exhibit remanent magnetism. Its center of mass is offset from its geometric center by 2 km towards

Earth. The Moon is tectonically dead and is tidally locked into a resonant orbital revolution around the Earth which equates to the Moon's axial spin (synodic day) of around 29 days. The sub-solar point remains within  $1.59^\circ$  of the equator throughout the lunar cycle, so high equatorial regions exhibit high solar inclination angles. The nearside equatorial sites visited by the Apollo missions were geochemically unusual with elevated concentrations of KREEP (potassium, rare earth elements, and phosphorus) elements resultant from impact ejecta from the formation of the 1200 km diameter Imbrium impact crater  $\sim 3.85\text{--}3.90$  Gyr ago. The Moon's surface is characterized by rugged highlands characterized by anorthosite rich in Ca and Al and younger smooth "maria" plains of basalt rich in Fe and Mg, the highlands representing the more ancient crust. The smooth maria are concentrated on the nearside facing the Earth. Due to constant meteoritic flux over the eons, the lunar surface is heavily scarred by impact basins and craters. In particular, the lack of atmosphere allows microtektitic bombardment which has pulverized the surface layer into a fine-grained regolith.

Lunar rocks are constructed from minerals and glasses that formed under negligible oxygen partial pressure and in the absence of water. Minerals are solid crystalline solutions. Only four minerals—plagioclase feldspar, pyroxene, olivine, and ilmenite—comprise over 98% of the lunar crust. The remaining  $<2\%$  is primarily potassium feldspar, metal oxide minerals (such as rutile  $\text{TiO}_2$ , and chromite  $\text{FeCr}_2\text{O}_4$  but little evidence of hematite or magnetite), metal iron grains, troilite  $\text{FeS}$ , zircon  $\text{ZrSiO}_4$ , and calcium phosphate. Feldspar is an aluminosilicate while plagioclase is a type of feldspar being a Ca-Na-aluminosilicate. Most lunar feldspars are of the plagioclase type which varies between albite ( $\text{NaAlSi}_3\text{O}_8$ ) and anorthite ( $\text{CaAl}_2\text{Si}_2\text{O}_8$ ). Anorthite is a Ca-rich form of plagioclase feldspar which is dominant on the Moon. Almost all lunar Al exists in plagioclase form. Pyroxene is a Mg-Fe-Ca silicate (e.g., enstatite  $\text{MgSiO}_3$ , wollastonite  $\text{CaSiO}_3$ , and ferrosilite  $\text{FeSiO}_3$  end members), clinopyroxene ( $\text{Ca}(\text{Mg,Fe})\text{Si}_2\text{O}_6$ ) is a pyroxene containing Ca (associated with mare basalts), while orthopyroxene ( $(\text{Mg,Fe})\text{SiO}_3$ ) is a pyroxene containing negligible Ca (associated with highland rock). Olivine is a Mg-Fe silicate whose composition varies between forsterite  $\text{Mg}_2\text{SiO}_4$  and fayalite  $\text{Fe}_2\text{SiO}_4$ . Most mare basalt olivine minerals are 80% forsterite and 20% fayalite. Almost all Fe and Mg are incorporated in pyroxenes, olivine, and ilmenite. Lunar rocks have a near constant ratio of Fe/Mn of 70. Lunar highlands are anorthositic due to the high incidence of the plagioclase feldspar mineral anorthite and small amounts of pyroxene and olivine. Lunar basalts of the maria are comprised mostly of silicates (olivines, plagioclase feldspars, clinopyroxenes). Lunar silicates are the most abundant minerals which include pyroxene ( $\text{Ca,Fe,Mg}_2\text{Si}_2\text{O}_6$ ), plagioclase feldspar ( $\text{Ca,Na}(\text{Al,Si})_4\text{O}_8$ ), olivine ( $\text{Mg,Fe}_2\text{SiO}_4$ ). Lunar oxides are the next most abundant minerals, particularly in the mare basalts which include ilmenite ( $\text{Fe,MgTiO}_3$ ), spinel  $\text{MgAl}_2\text{O}_4$ , chromite  $\text{FeCr}_2\text{O}_4$ , ulvöspinel  $\text{Fe}_2\text{TiO}_4$ , and hercynite  $\text{FeAl}_2\text{O}_4$ . In the northwest nearside of the Moon lies the Procellarum KREEP Terrane which is enriched in pyroxene rather than plagioclase with enrichment in K and rare earth elements. Silica minerals  $\text{SiO}_2$ , such as quartz, and most sulfide minerals are rare on the Moon. The paucity of silicate minerals due

to the lack of hydrothermal precipitation of silica yields little granite (lunar granite does not contain mica or amphibole). However, the silica minerals concentrate in association with KREEP elements. Since sulfides are rare, consequently elements Cu, Zn, As, Se, Hg, Ag, and Pb are in very low abundance. Water-containing minerals such as clays, micas and amphiboles are absent—most ore-forming processes on Earth are based on water so ore concentrations do not exist on the Moon.

Lunar water has been detected in the hydrous mineral apatite, a constituent of mare basalts and highland anorthosite [44]. Hydrogen isotope analysis indicates that much of this water may originate from cometary delivery. The Moon is expected to have water ice at its poles in permanently shadowed craters where temperatures are  $\sim 100$  K acting as cold traps. Volatiles including water would have been delivered to the Moon by cometary impacts over the eons. Characterization of any water ice deposits is one major rationale for robotic rover missions in order to support such human exploration. The U.S. lunar orbiter missions Clementine (1994) using S-band bistatic radar and Lunar Prospector (1998) using neutron spectroscopy mapped the lunar farside and polar regions and their instruments suggested that  $\sim 10^9$  tonnes of water ice may reside in permanently shadowed craters at both poles—these data were indirect in the form of radar reflectivity and hydrogen signatures, respectively, and the form of the “water ice” is still unknown until further measurements are made (other possibilities include methane ice or hydrogen impregnation). The Indian Chandrayaan-1 spacecraft’s mini-synthetic aperture radar (SAR) suggest the existence of water ice at the lunar North Pole. The Lunar Reconnaissance Orbiter (LRO) mission (2009) performed orbital surveying of the lunar South Pole and worked in tandem with LCROSS (Lunar Crater Remote Observation and Sensing Satellite). LCROSS impacted the lunar South Pole region ejecting a plume of debris and volatiles which was analyzed spectrally by the LRO. The measurements suggest the existence of molecular hydrogen (amongst other things), possibly derived from water ice estimated to comprise 5.6% of the floor of the shadowed crater Cabeus that was targeted. It is not clear if Cabeus is unusually enriched as might be expected from a former cometary impact site or representative of permanently shadowed craters. Nevertheless, the existence of water ice has yet to be confirmed with confidence. Confirmation of lunar water deposits, locating mineral supplies and the creation of topographic maps are high priorities using high-resolution cameras, laser altimeters, IR spectrometers, X-ray/gamma-ray spectrometers for future human mission scenarios. The existence of water resources on the Moon will enable support of human lunar missions at much lower cost particularly for colonization.

The solar wind and cosmic rays have implanted volatiles into the lunar regolith. Solar wind implantation of gases is enhanced within the polar regions of the Moon by virtue of its low temperature  $< 100$  K reducing their desorption rate which more than compensates for lower solar wind flux at high latitudes [45]. This suggests that the polar regions are the most promising sites for extraction of both hydrogen (which may be molecular gases or water ice) and He-3 with a much reduced concentration of  $[\text{He-3}] = 3(0.025)(4 \times 10^{-4})H_{\text{max}}$ . The Moon is thus the

nearest source of He-3 (rare on Earth) for clean nuclear fusion. Such solar wind–implanted gases may be released by heating to 700°C which may be possible with lunar infrastructure development. In situ resource utilization (ISRU) at the lunar South Pole has been proposed to exploit water ice deposits. Water deposits offer the prospect of life support and the manufacture of propellant, oxidizer, and fuel cell reagents. Water is the most critical commodity for life support as well as providing a source of oxygen on electrolysis. Such water deposits are expected to lie at shallow depths  $\sim 1$  m [46]. Although deep drilling requires human intervention, sample collection and scientific instrument deployment can be performed robotically. The hydrogen distribution as measured by Clementine and Lunar Prospector was limited to  $\sim 0.5$ –10 km/pixel, insufficient for targeting sites for landing (but the U.S. Lunar Reconnaissance Orbiter launched in 2009 is designed to investigate potential target sites for landing). Lunar mineralogy also offers a promising in situ resource of oxygen, silicon, iron and titanium in high-yield concentrations through carbothermic reduction. Such in situ resource capabilities offer the possibility of long-term commercial potential.

There are a number of science objectives that make the Moon an attractive target [47]. The Moon has scientific interest on its own merits with a rich geology. Regions such as impact crater interiors exhibiting  $\sim 30$  K temperatures will trap and retain water ice and other volatiles derived from cometary and asteroid impacts over the eons. Given the high priority of characterizing the water deposits at the polar regions, the South Pole Aitken basin is favored for robotic rover missions. The South Pole Aitken crater ( $180^\circ\text{W}$ ,  $57^\circ\text{S}$ ) on the farside is 2,250 km in diameter. This makes it the largest impact crater in the Solar System. It is the oldest and deepest impact basin on the Moon, formed  $\sim 3.9$  Gyr ago during the terminal cataclysm phase of early solar system accretion. It has an altitude which varies from 6 km above the local horizontal (e.g., Malapert Mountain  $\sim 120$  km from the South Pole) to  $-5$  km depth below the local horizontal (i.e., a topographic profile of 13 km range). Its depth suggests that the impact penetrated the crust and excavated lunar mantle material, which has not so far been sampled. The mass of the impactor that formed the South Pole Aitken crater is estimated at  $1.5 \times 10^{19}$  kg. The surface is covered with regolith of pulverized rock and dust. Areas of the basin floor are in permanent shadow and so may have trapped volatiles. The following analysis of potential landing sites and rover missions has been developed by Philip Stooke at the University of Western Ontario. The 39 km diameter Shoemaker–Faustini crater ( $87.3^\circ\text{S}$ ,  $77.0^\circ\text{E}$ ) is a promising target with  $[\text{H}] = 0.17\% = 1,700$  ppm and  $[\text{He-3}] = 10^{-7} \sim 100$  ppb where the temperature is estimated at  $\sim 100$  K. This was the primary landing site for the Hopper sample return mission concept. However, there are other possibilities.

A cross section through the South Pole Aitken basin exhibits a stair-like topography (Figures 2.3 and 2.4). Three concentric rings may be defined through the Aitken basin. Ring 1 has a diameter of 2,400 km and the elevation drops sharply by 3–4 km. Ring 2 has a diameter of 2,100 km and the elevation drops by 2–3 km. Ring 3 has a diameter of 1,500 km enclosing the deepest parts of the basin with a sharp drop of 2–3 km depth on transition to rings 2 and 3. Now, a good



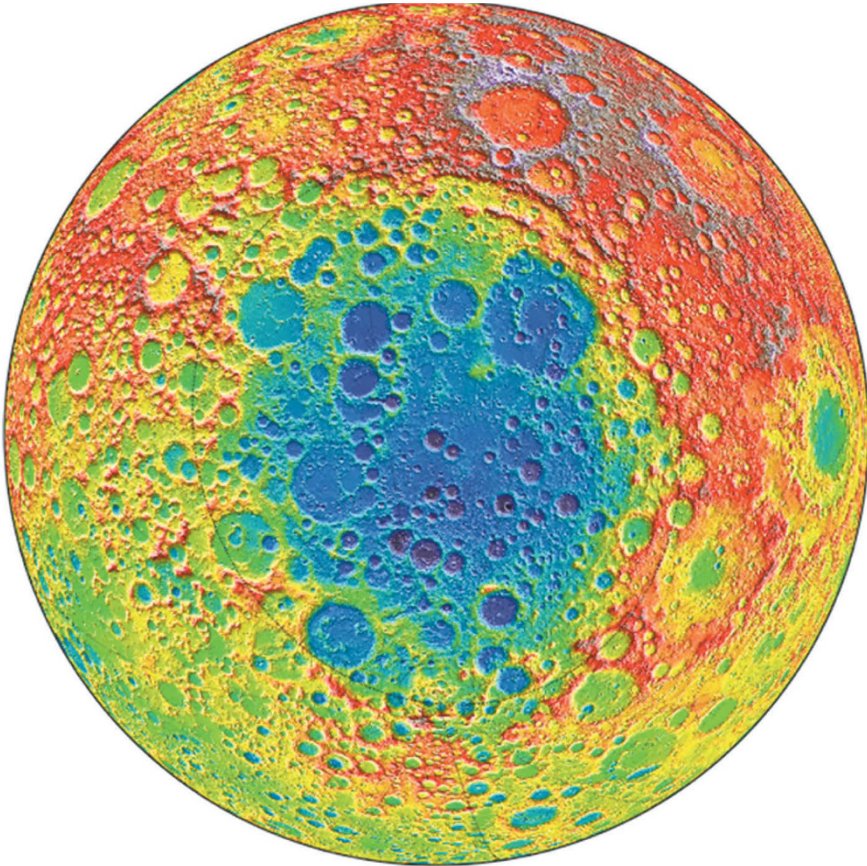


**Figure 2.3.** South Pole Aitken (SPA) basin [credit NASA].

landing site requires: (i) good illumination for solar power generation; (ii) good view to Earth for communication; (iii) feasible rover routes to permanently dark crater regions; (iv) accessibility for orbital imaging; (v) reasonably rock-free and flat terrain. As the Moon's axis is tilted  $5^\circ$  from the Earth–Moon ecliptic plane, communications from the Moon to Earth require a minimum elevation of  $5^\circ$ . Polar landing sites offer a line of sight to Earth with a maximum azimuth  $7^\circ$  above the horizon during midsummer with an azimuth variation of  $\pm 5.5^\circ$  over a lunar day. These margins are too severe to guarantee continuous communications (accounting for topographic obstruction) suggesting the need for a communications relay satellite in lunar orbit. The Malapert Mountain peak ( $86.0^\circ\text{S}$ ,  $2.7^\circ\text{E}$ ) has a continuous line of sight to Earth but  $<74\%$  illumination. Older craters at the South Pole exhibit rounded edges with thick ejecta blankets. However,



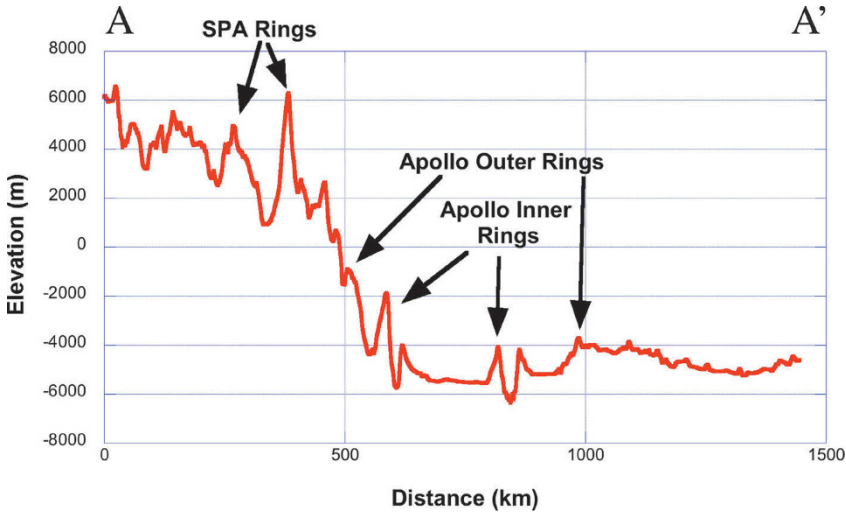


**Figure 2.4.** Cross section through northern part of SPA basin [credit NASA].

boulders  $\sim 1$  m diameter may be present at and nearby the rim but may reach as much as 70 m in diameter (this will impact rover operations). Younger craters with steeper sides  $\sim 20\text{--}25^\circ$  will present greater challenges to rover traction suggesting that the traditional rocker-bogie six-wheeled chassis design will provide insufficient traction. This favors a tracked solution such as a larger version of Nanokhod or the elastic loop mobility system (ELMS). Near the lunar poles, local topography will obscure solar incidence to certain locations. There will be topographically elevated regions that will be illuminated by the Sun near-continuously—these may lie in close proximity to the permanently shadowed regions. There are several promising regions where high illumination (86% of the year) occurs in close proximity to permanently shaded craters [48]: (i) Point A on the rim of the Shackleton crater ( $89.68^\circ\text{S}$ ,  $166.0^\circ\text{W}$ ); (ii) Point B on a ridge close to the Shackleton crater ( $89.44^\circ\text{S}$ ,  $141.8^\circ\text{W}$ ); (iii) Point C on the rim of the De Gerlache crater ( $88.71^\circ\text{S}$ ,  $68.7^\circ\text{W}$ ); (iv) Point D ( $99.79^\circ\text{S}$ ,  $124.5^\circ\text{E}$ ) on a ridge from the Shackleton crater rim along the  $120^\circ\text{E}$  longitude line. The most illuminated regions occur on the western rim of the Shackleton crater (Figure 2.5).

A, B, and C are the most illuminated regions with a minimum of  $>70\%$  illumination—A (on the rim of Shackleton crater) and B are 10 km apart and both are collectively illuminated for 98% of the time but no single spot is continuously illuminated (peaks of eternal light). Point D offers illumination  $>86\%$  of the year, and during the summer it is illuminated continuously for 5 months while individual eclipses during the 7-month eclipse season are short. However, nearby access to permanently shadowed regions to detect volatiles is necessary (within 10 km preferably). The proposed Hopper lander which hops between three sites

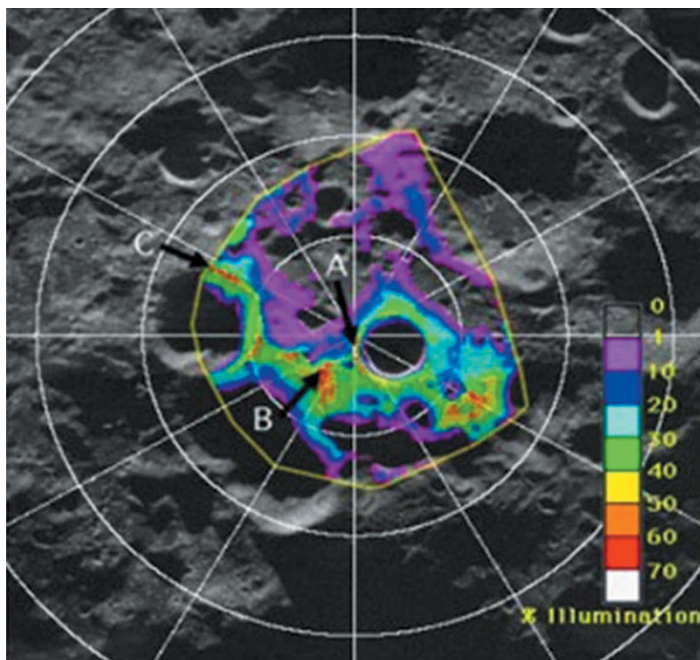


**Figure 2.5.** The 20 km diameter by 3 km deep Shackleton crater indicating % solar illumination [credit NASA].

50 m apart using thrusters would be insufficient to locate permanently frozen water ice deposits given the separation of peaks of eternal light and permanent shadow. A lunar rover must have access to nearby, permanently shadowed craters. The most appropriate landing sites are selected on the ejecta blankets of the Shackleton and de Gerlache craters.

Sites 1 and 2 on the Shackleton rim provide potential access to the interior of the 20 km diameter and 3 km deep Shackleton crater. However, Shackleton is relatively young, implying steep walls and reduced volatile inventory. The exterior slope of the Shackleton crater is less severe than its internal slope. Sites 3, 5, and 6 offer short drives into nearby small craters but small craters are likely to have limited volatile inventory. Site 4 requires a 20 km traverse into an older crater with both shallow interior slopes and a likely significant volatile fraction. Communication may be maintained from the lander at site 4. As the rover traverses, it will lose line-of-sight communication with the lander implying the need for relay deployment (mass expensive) or through an orbiter satellite. Site 7 offers several routes to the de Gerlache crater. The baseline landing site is site 4 implying the need for significant mobility for outward and return trips from the lander (Figure 2.6).

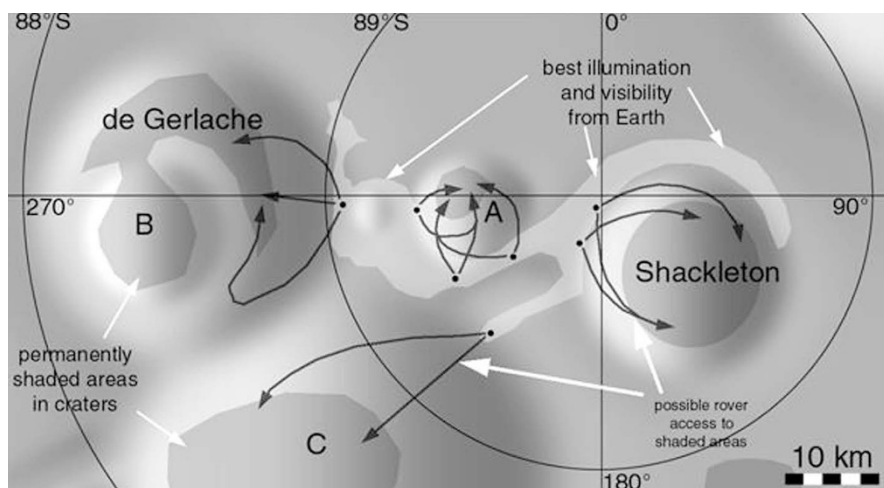


**Figure 2.6.** Potential rover routes from peaks of eternal light [credit Phil Stooke, University of Western Ontario].

The lander must land at an eternally sunlit region for constant solar power adjacent to a permanently shaded region within the Shackleton crater with a high-mobility rover on board. The baseline rover traverse will be highly challenging—20 km each way over extremely rugged terrain within the Shackleton crater with high vertical variation. There will be limited and variable solar illumination for the rover. The traverse is assumed to be restricted by the 14-day daytime window, implying a minimum speed of under 3 km/24 h day. If operational around the clock, this imposes a minimum speed of 120 m/h. This does not include the scientific investigation at the target site. This will be highly challenging.

As an example, the proposed lunar resource prospector/RESOLVE (regolith and environment science and oxygen and lunar volatile extraction) mission for 2018 is an ISRU mission to locate near-subsurface volatiles, such as water, extract and analyze samples of such, and demonstrate chemical processing of lunar regolith at a shadowed region near the lunar South Pole. The selected site requires periods of sunlight to allow the use of 250 W solar panels for energy (supported by 3.5 kWh rechargeable batteries) and continuous line-of-sight visibility to Earth (Antarctica stations) yet provide access to shadowed regions with high hydrogen concentration and high ice stability. The lunar resource prospector is based on a 243 kg robotic lunar rover (including payload) for a surface mission of 1–3 km over 5–7 days to the Cabeus crater (85.75°S, 45°W) [49]. The landed mass is 1,285 kg while the launch mass on the Atlas V is 3,476 kg. The 72 kg integrated RESOLVE payload comprises four subsystems: (i) a sample site selection system consisting of a neutron spectrometer and near-infrared spectrometer to locate

hydrogen/water sources; (ii) a sample acquisition and transfer subsystem comprising a 1 m drill/auger and core transfer mechanism to perform three to five 1 m drill cores; (iii) the oxygen and volatile extraction node (OVEN) for sample chemical processing consisting of a sample heating reactor oven to 900°C; and (iv) the lunar advanced volatile analysis (LAVA) system for evolved volatile characterization comprising a gas chromatograph–mass spectrometer (GCMS) and a water capture device involving a condensation chamber. A 1 m core is divided into eight segments, which are to be processed. They are to be heated to 150°C for volatile extraction and to 900°C with hydrogen for hydrogen reduction to extract oxygen. The evolved volatiles are to be analyzed by the GCMS.

Lunar dust is ubiquitous and adheres to everything due to its frictional and electrostatic properties. The fine-grained dust is levitated by solar ultraviolet radiation during the day and by solar wind flux during the night [50]. Lunar soils have increasing abundances of agglutinate glasses and nanophase metallic iron content with decreasing size (Gaussian average size is 3.0  $\mu\text{m}$ ) [51]. There are a significant number of particles <2.5  $\mu\text{m}$  which are regarded as toxic to the respiratory system. Lunar soil has an average aspect ratio of 0.7 and exhibits angular jagged shapes making it highly adhesive. This presents a major problem for extended lunar operations and will require aggressive mitigation techniques [52]. Dust mitigation to prevent settling of dust particles and their adhesion by van der Waal forces onto solar arrays, thermal radiators, and optical surfaces may be achieved through several mechanisms—vibromechanical, (electro)magnetic, and electrostatic removal. Although magnetic approaches are simple [53], electrostatic ones are favored as the most effective [54–56]. Lunar soil of all particle sizes is also a significant problem for mechanical components such as motors and gears used on rovers, manipulators, and drills. For robotic applications, rotary seals must be used as the primary or secondary mechanism for dust mitigation. Rotor/stator airgap, motor alignment, brush/commutator wear, gearing friction and meshing, sheave seating, connector coupling integrity, bearings, and motor temperature are highly susceptible to dust contamination. Rotary seals are used for sealing between moving parts. While static seals rely on solid–solid contact, rotary seals require fluid lubrication, usually hydrocarbon oil of low viscosity. Moving parts require lubrication to minimize friction and wear. Most wet lubricants operate on the basis of their viscosity and thin-film adhesion. Wet lubricants are made of petroleum-based and synthetic chemicals. For space use, PTFE seals are most appropriate as a dry lubricant which is resistant to temperature excursions and has high chemical stability. Teflon O-ring seals have been tested and found to be inadequate for high-dust environments (modeled with angular silica dust) [57]. Magnetic fluid rotary seals can be used in vacuum and low pressures offering zero leakage for fluid sealing [58]. Two opposing magnets create a magnetic circuit and contain a ferrofluid. Ferrofluids are colloidal suspensions of paramagnetic particles of 10 nm diameter within a fluid which imparts paramagnetic behavior to the fluid as a whole. The application of magnetic fields allows control of such fluids which can be used to seal two regions. This makes them ideal for rotary seals in motors.

## 2.2 MARS

The Martian terrain comprises five major divisions: (i) highland rock; (ii) lowland rock; (iii) volcanic regions; (iv) channel systems; (v) polar regions (Figure 2.7). The northern hemisphere is flat with an average elevation of  $-1$  to  $-3$  km compared with the mountainous southern hemisphere with an average elevation of  $+4$  km. The northern hemisphere has more moderate seasons than the southern hemisphere—the mean daily temperature ranges from 215 K at the equator to 150 K at the poles. At the equator, night-time temperatures drop to 150 K and reach 290 K at noon, but Martian soil remains close to the average of 215 K. The most obvious features are water-cut channels and flood basins etched across the Martian surface. The heavily cratered ancient ( $\sim 3.5$ – $4$  Gyr old) highlands of the southern hemisphere are characterized by river valley networks contrasting with the smoother, younger low-lying plains of the northern hemisphere with ancient shorelines separated by an equatorial region of canyons and volcanoes of the Tharsis plateau. The Martian crust is 40 km thick in the northern hemisphere and 70 km thick in the southern hemisphere. The crust is thickest under the Tharsis volcanoes and thinnest at the giant Hellas impact basin in the southern hemisphere. The main volcanic regions of Mars are Tharsis and Elysium. Tharsis at a mean altitude of 10 km at the equator represents the region where tectonic faults and volcanoes are generated. The Tharsis bulge was created 3.7 Gyr ago but the caldera floors of the Tharsis mountains including Olympus Mons were formed only 100–150 Myr ago indicating recent volcanic activity.

Martian history is divided into three major epochs—Noachian (southern highlands), Hesperian (northern lowlands), and Amazonian (volcanic regions).

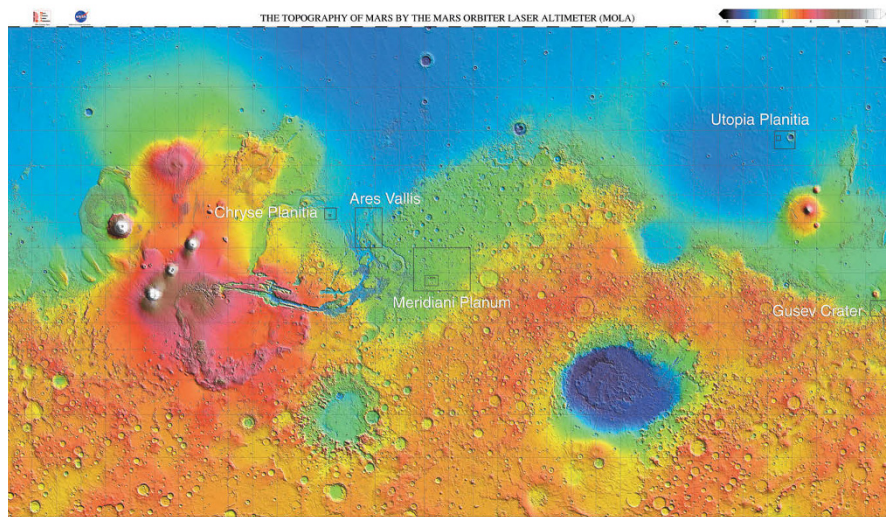


**Figure 2.7.** Topographic map of Mars generated from MOLA data [credit NASA].

The boundaries are calibrated from the lunar cratering record—Noachian/Hesperian (3.5–3.7 Gyr), Hesperian/Amazonian (2.9–3.3 Gyr). Of its 20 large volcanoes, Mars sports the largest shield volcano in the solar system—Olympus Mons east of Tharsis—with a height of 22 km, caldera diameter of  $60 \times 90$  km, and depth 3 km. The Martian surface has been substantially altered by the action of liquid water in two phases—an early epoch when the valleys were formed and a later epoch when outflow channels were formed, especially at the interface between northern lowland and southern highlands where there is an elevation discontinuity of around 5 km [59–61]. There is evidence of substantial quantities of water ice 1–2 m below the surface regolith of Mars at latitudes exceeding  $50^\circ$  sufficient to flood the planet to a depth of 500 m. Further near-surface water is indicated at much lower latitudes though its form is not known (e.g., chemically or physically bound in minerals). Adsorbed water has much stronger bonds due to van der Waal forces. The Viking experiments heated soil samples up to temperatures of  $500^\circ\text{C}$  to release water of hydration indicating an integrated average of 0.2% water for all regolith. The discovery of both goethite and jarosite by the MERs indicate chemically bound water in minerals on the Martian surface. The outflow channels and valley networks on Mars have long indicated the presence of liquid water on the Martian surface during different epochs. The outflow channels are large fluvial features formed by catastrophic flooding in the northwest and Chryse regions while the older valley networks were formed by surface runoff fed by groundwater seepage [62]. Valley networks in the southern highlands may have formed near the end of the heavy bombardment phase  $\sim 3.5$  Gyr ago, which would have maintained clement conditions due to hot ejecta [63]. Groundwater sapping is caused by geothermal melting of near-surface ice. There would be a net migration of groundwater ice from warm equatorial regions where water is unstable to sublimation to the polar regions where it is more stable as subsurface permafrost at shallow depths  $< 1$  m [64]. Although this subsurface ice is most stable at shallow depths poleward of  $40^\circ$  latitude, its incidence is more widespread. The largest outflow channel is Kasei Vallis. Outflow channels were dominant during the Hesperian but some may have originated during the Amazonian.

The valley networks throughout the ancient heavily cratered terrains which formed after the late heavy bombardment suggest that the early Martian atmosphere was capable of supporting a hydrological cycle in a warm, wet climate (1–5 bar  $\text{CO}_2$ ) during the Noachian epoch [65]. A thick  $\text{CO}_2$  greenhouse atmosphere of  $\sim 1$  bar would have been insufficient by itself to maintain warm enough conditions for liquid water. However, the formation of  $\text{CO}_2$  ice clouds may have trapped thermal radiation in the surface [66]. Alternatively, greenhouse gases  $\text{H}_2\text{O}$  and  $\text{SO}_2$  (the latter being a minor constituent supplied by periodic volcanic emissions but which inhibits the formation of  $\text{CO}_2$  cloud condensation) ensured stable bodies of liquid water on the surface [67–69].  $\text{CO}_2$  has a strong vibration absorption band at  $15\text{ }\mu\text{m}$  and several weaker less significant bands near 9 and  $10\text{ }\mu\text{m}$ . Water vapor has rotational absorption bands longward of  $20\text{ }\mu\text{m}$  and a weak continuum absorption band between 8 and  $12\text{ }\mu\text{m}$  well above 273 K.  $\text{SO}_2$  has vibrational absorption bands near 7, 9, and  $19\text{ }\mu\text{m}$  and rotational transitions long-



ward of  $40\text{ }\mu\text{m}$ .  $\text{NH}_3$  has vibration absorption bands at  $10\text{ }\mu\text{m}$  and a weaker line at  $16\text{ }\mu\text{m}$ .  $\text{CH}_4$  has an absorption peak at  $7.7\text{ }\mu\text{m}$ . Reduced gases  $\text{CH}_4$  and  $\text{NH}_3$  are unstable to solar UV action, however. For  $\text{CO}_2$  and  $\text{CH}_4$ , absorption longward of  $20\text{ }\mu\text{m}$  is only important at higher pressures. There exist younger ( $<2.5\text{ Gyr}$  old) valleys in the Tharsis region (Alba Patera) which were formed by local surface runoff while the Martian climate was similar to the present day [70]. There is evidence that the northern lowlands indicate ancient equipotential shorelines of a large ocean below which the topography is unusually smooth and flat with an average depth of  $3.8\text{ km}$  below the geoid and a capacity of  $1.4 \times 10^7\text{ km}^3$  [71]. This ancient ocean—Oceanus Borealis—may have persisted up to the late Hesperian. Outflow channels empty into the northern lowlands from Chryse and Amazonis. The northern regions include the Elysium plains. The tectonics of the Tharsis region has not changed appreciably since the late Noachian though it may have been the source of episodic flooding on the northern plains.

The Valles Marineris rift canyon has a length of  $4,000\text{ km}$ , a width of  $65\text{ km}$ , and a depth of  $8\text{--}10\text{ km}$  formed with the creation of Tharsis (Figure 2.8). Its layered deposits suggest large amounts of hydrated sulfate salts indicating that catastrophic outflows have occurred triggered by volcanic heat sources. During the late Noachian and early Hesperian, Valles Marineris underwent radical tectonic activity generating outflow channels with the Valles Marineris structures forming during the late Hesperian and early Amazonian. However, volcanic and tectonic activity have continued until the present day (within the last  $10\text{ Myr}$ ) indi-

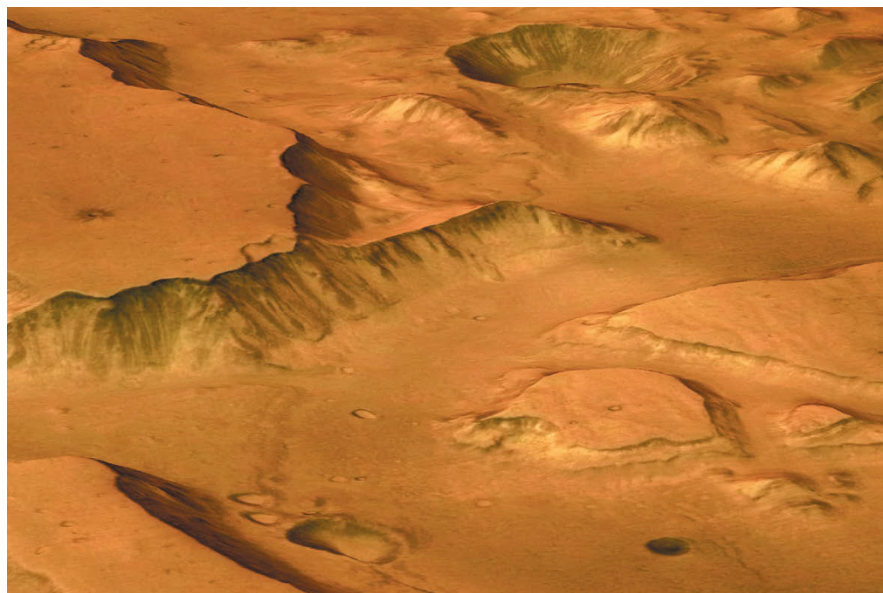


**Figure 2.8.** Valles Marineris [credit NASA].

cated by features in the Tharsis Montes region and evidence of recent water flows—gullies, floods, polar layered northern ice cap [72]. There is evidence of intermittent volcanism within the last 100 Myr at Tharsis and Elysium—Cerberus Fossae to the southeast of Elysium Mons indicates magma flows within the last 3 Myr—this is within the approximate cool-down timescale for magma chambers. Furthermore, this is believed to be the source of the lowland flooding near the north side of the equator indicated by the fragmented plates believed to be ice rafts overlain by volcanic ash and dust erupted from Cerberus Fossae. Exposed Martian gulleys on pole-facing steep crater walls between 30–70° latitudes in both hemispheres indicate recent erosion by liquid water flows within the last ~1–5 Myr [73]. This indicates that there are multiple layers of ice deposits from 0.2 to 1.0 km depth. This recent activity is primarily due to a recent obliquity change to high obliquity exceeding 35° (within the last 5 Myr) for  $\sim 10^5$  yr. This would have generated sublimation of carbon dioxide and water to give atmospheric pressures >25 mbar generating the precipitation of snow which can flow as glaciers.

Subsurface ice is indicated by the existence of landforms resulting from viscous deformation such as fluidized ejecta craters which requires a minimum of 28% ice at 1 km depth in the permafrost (with 40% ice near the surface) [74]. This implies a global water inventory to a depth of 1 km. Most of the planet, apart from the equatorial regions, has ground ice to high depths. The cryosphere is stable at depths of 3–5 km at the equator to 8–13 km at the poles below which liquid water may exist. Ground ice is unstable at shallow depths at latitudes below 40° where ice sublimates. The freezing point of water may be depressed by salts increasing the latitude range of water melting. Dilute aqueous solutions of  $\text{H}_2\text{SO}_4$  can depress the freezing point of water by 70°C. The seasonal change in polar deposits on Mars is primarily due to carbon dioxide ice. However, the Martian North Pole is comprised mostly of water ice with variable amounts of dust while the southern cap is also primarily water ice with little dust. Polar ice and permafrost may potentially yield ancient bacteria (a few million years old or so) and gases such as methane, ammonia, hydrogen sulfide, sulfur oxides, and nitrogen oxides. The Martian poles comprise ice/dust layers over  $10^6 \text{ km}^2$  with a thickness of 3–4 km which varies seasonally but which has existed for  $10^5$ – $10^8$  yr. They possess extensive ground ice in the upper layers of the soil, probably overlying deeper older ice. In particular, the South Pole represents heavily cratered ancient terrain. The large-obliquity cycles of Mars varying by 45° with periods of  $10^5$ – $10^6$  yr suggest that the poles receive more sunlight at high obliquity. The current Martian obliquity is 25.2° from the plane of the Sun but varies substantially over a few million years. The obliquity of Mars' spin axis has varied chaotically from 0–60° while Mercury and Venus are tidally stabilized by the Sun and the Earth is tidally stabilized by the Moon [75, 76]. For Mars, spin axis precession is driven by solar torques while orbit precession is caused by perturbations by other planets. The Martian obliquity oscillations due to spin–orbit resonance over  $\sim 10^6$ – $10^7$  years drive the Martian climate [77]. In the past 20 Myr, Mars' obliquity was closer to 45° which would have warmed higher latitudes and vaporized ground ice near the surface. It can lean as far as 60° generating a thick

atmosphere due to polar ice evaporation. Periodic catastrophic outflows indicate enormous flood releases  $\sim 10^6$ – $10^8$  m<sup>3</sup>/s. These short episodes of regional flooding may have persisted for  $\sim 10^3$  yr rather than  $\sim 10^6$  yr. At greater planetary inclinations of 40–60°, greater sunlight evaporates the northern polar water ice which migrates to lower latitudes, increasing atmospheric pressure  $\sim 30$  mbar, greenhouse effect, and surface temperature [78]. This has a direct effect on the Martian climate including generating precipitation from a water-saturated atmosphere at low latitudes. This may cause permafrost to warm to a thermal damping depth of

$$d^2 = \frac{KT}{\pi}$$

where  $K$  = thermal diffusivity and  $T$  = oscillation period. This suggests that drilling to a depth of 1 km is required to access undisturbed permafrost. Such ancient permafrost is reckoned to be the most likely candidate for preservation of fossilized remains of biological organisms on Mars [79]—this permafrost is around 3.5 Gyr old compared with Siberian permafrost (5 Myr old) and Antarctic permafrost (8–20 Myr old). Martian permafrost temperatures are much lower ( $< -90^\circ\text{C}$ ) possibly allowing longer preservation of biological viability. However, the radiation flux from U, Th, and K decay of 0.2 rad/yr makes such long-term survival unlikely. There is substantial evidence of glacial forms over a wide range of longitudes, latitudes, and altitudes including equatorial regions—this suggests that the Martian climate has changed relatively recently (within the last 5 Myr). There are glacial features indicating recent surface ice at equatorial regions as well as polar features resembling eskers and karsts [80]. This provides support for obliquity-driven climate in which the stability of surface water varies with time. The near-surface soil across much of the Martian subsurface may be 50% water ice.

Heat loss from the Martian interior caused a decline in volcanic activity while water evaporated as the Martian atmosphere thinned. The Martian climate has undergone significant evolution. It may have been lost during the heavy bombardment phase due to impact erosion [81]. Alternatively, it occurred subsequently by a combination of solar wind-induced sputtering, Jeans escape of H, and photochemical loss of N and O [82]. The history of Martian volatiles is indicated by measurements of D/H,  $^{18}\text{O}/^{16}\text{O}$ , and  $^{38}\text{Ar}/^{36}\text{Ar}$  indicating that there was a massive early loss of Martian atmosphere [83]. There is a large deuterium enrichment D/H in the atmospheric water vapor indicating major loss of H equivalent to a global ocean thickness of 100 m. Martian atmospheric density is low at 0.02 kg/m<sup>3</sup> having been sputtered over the eons by the solar wind after the freezing of the Martian core (which also provides an explanation for the lack of detected carbonate deposits). The atmospheric pressure on Mars is around 6–7 mbar on average but varies seasonally by 25% due to the condensation/sublimation of carbon dioxide at the poles. The average wind velocity at the surface is 2–9 m/s but can gust up to 60 m/s. The largest dust storms begin in southern spring as Mars heats up, sometimes encircling the whole planet. A typical dust storm is 200–300 m in diameter and tends to occur at 2–3 PM local time. During summer the surface winds are low ( $\sim 2$ –7 m/s) but increase to 5–10 m/s during autumn and rise to

20–30 m/s during dust storms. The NASA Ames Mars general circulation model indicates a 6-day average oscillation in atmospheric heating rates generating localized dust storms in the northern spring in lowland regions [84]. These dust devils are generated by local surface heating generating plumes of warm air in the surrounding cooler air which then circulate in convection cells.

In situ analysis of Martian rock indicates basaltic and andesitic rock enriched in oxides and sulfides. The dominant silicate minerals are olivine, plagioclase feldspars, pyroxenes (clinopyroxene and orthopyroxene in Hesperian and Noachian deposits, respectively), and quartz mixed with Ti–Fe oxides. Most Martian meteorites are basalts with pyroxene–olivine secondary minerals. Basalt dominates the southern hemisphere while andesite is common in the northern hemisphere. This follows a well-defined pattern of igneous rock melting separating out the silica content. Mantle material is primarily olivine which, if melted, forms basalt. Basalt if melted yields andesite, melted andesite yields dacite, and dacite when melted yields granite. Only miniscule amounts of granite exist on Mars. It appears that Mars has been host to transient lakes which have undergone repeated cycles of drying and wetting generating acidic salt flats built from layers. The Meridiani plains also exhibit distinctive arc wave patterns indicative of shallow-water lakes. Hematite and goethite are common iron (oxy)hydroxides found on Mars. In Meridiani Planum, Opportunity discovered “blueberries” of localized gray hematite ( $\alpha\text{-Fe}_2\text{O}_3$ ) deposits formed in water associated with evaporitic deposits. Mineral grain size distribution is consistent with water deposition rather than wind. Goethite ( $\alpha\text{-FeOOH}$ ) is a hydrated iron mineral commonly associated with hematite suggesting aqueous formation. Ferrihydrite ( $5\text{Fe}_2\text{O}_3 \cdot 9\text{H}_2\text{O}$ ) is the anhydrous precursor to hematite and goethite—goethite is formed at low temperature and low pH while hematite is formed at higher temperature and higher pH. The discovery of the mineral jarosite suggests that water was acid and briny. Martian mineralogy is reviewed in Chevrier and Mathe (2007) which stresses the importance of the formation of sulfate salts by acidic solutions due to water evaporation and hydrothermal processes indicated by SNC meteorites [85]. Phyllosilicates—clays, serpentine, and talc—are the common derivatives of water action on silicates. Nakhilite meteorites indicate smectite–illite clay mineral veins and other evaporite minerals such as gypsum and salts within olivine clinopyroxenites [86]. Clay minerals have been detected in the oldest regions of Mars indicative of aqueous processes. Endeavour crater contains clay minerals that require near-neutral pH to form. Acidic solutions destroy carbonates and inhibit the formation of clays. Rudimentary dating of K-40/Ar-40 ratios by the Curiosity rover’s sample analysis at Mars (SAM) instrument suggests that clay deposits were laid down as recently as 80 Myr ago. Maghemite is believed to be a constituent of Martian rock varnish resulting from weathering under Martian conditions. Magnetization in Martian rocks is dominated by magnetite ( $\gamma\text{-Fe}_3\text{O}_4$ ), titanomagnetite ( $\text{Fe}_{3-x}\text{Ti}_x\text{O}_4$ ), and maghemite ( $\gamma\text{-Fe}_2\text{O}_3$ ). The soil has high Fe and S content but low Si and Al content compared with terrestrial references. Fe is generally in the  $\text{Fe}_3\text{O}_4$  oxide and oxyhydroxide form. The high Cl and S content suggests the presence of soluble sulfate salts. Kieserite ( $\text{MgSO}_4 \cdot \text{H}_2\text{O}$ ), gypsum ( $\text{CaSO}_4 \cdot 2\text{H}_2\text{O}$ ), and

epsomite ( $\text{MgSO}_4 \cdot 7\text{H}_2\text{O}$ ) have been identified, which typically comprise over 50% bound water. High sulfate abundances are derived from sulfide minerals (such as troilite  $\text{FeS}$ ) in basalts by acid aqueous conditions. However, the existence of adjacent olivine deposits suggests that the aqueous conditions were short lived. Jarosite (hydrated iron sulfate mineral  $(\text{K}, \text{Na}, \text{H})\text{Fe}_3(\text{SO}_4)_2(\text{OH})_6$ ) has been identified on the Martian surface and is indicative of aqueous deposition. Hydrothermal processes are generally implied—Rio Tinto in Spain may be representative in which jarosite and iron oxides are deposited in acidic conditions under which acid-tolerant organisms thrive. Martian soil appears to be saturated in the salt perchlorate, such as  $\text{Mg}(\text{ClO}_4)_2$  which are found only in arid environments on Earth. Perchlorate salts can significantly reduce the freezing point of water providing one possible explanation for groundwater runoff. Perchlorates may be used as an energy source when coupled to a reduced reagent in the presence of water (ammonia perchlorate is used as an oxidizer in heated rocket fuel). One explanation for the Viking results was that when heating soil to release organics, perchlorates become powerful oxidizers. It was originally assumed that chlorinated organic molecules were the result of cleaning agents used to clean the Viking spacecraft. However, perchlorates may be induced through UV photochemistry at the surface of the soil which diffuses into the subsurface. This diffusion in combination with the UV radiation into the near surface would destroy any organic materials and any biomarkers. The predicted large-scale precipitation of carbonates such as siderite ( $\text{FeCO}_3$ ) derived from an earlier thicker atmosphere have yet to be identified (detectable with signatures near 2.5, 4, and 7  $\mu\text{m}$ ). Low concentrations <5% of carbonate—hydrated magnesium carbonates—have been detected in the soil but their paucity requires explanation. One possibility is that their low solubility means that they are overlain by more soluble minerals such as sulfates. Alternatively, the early Martian atmosphere included volcanically outgassed greenhouse gases  $\text{SO}_2$  and  $\text{H}_2\text{S}$ . Together with ferric iron in solution, this would have created an acidic ( $\text{H}_2\text{SO}_4$ ) oceanic environment and inhibited siderite formation, the first carbonate mineral to precipitate from solution [87, 88]. Soluble sulfur-bearing minerals result in acidic solutions which destroy carbonates. There is evidence in support of weathering under low pH (acidic) conditions [89].

The primary geological objective is to find sedimentary deposits which have been found across large depression areas of the Martian surface—craters, canyon floors, central plains, etc. Layered terrain which is widespread on Mars provides evidence of stratigraphic sedimentary deposition and of intermittent and ancient water flows which created this stratigraphic layering (Figure 2.9). In many impact craters (in particular, those with well-defined rims) there is evidence of standing bodies of water (e.g., the 1,000 km diameter Argyre basin appears to have been filled with water).

The search for evidence of water on the Martian surface is the primary scientific goal because of its implications for Martian life early in its history [90]. During the wet Hesperian period, conditions may have been suitable for the origin and evolution of microbial life. Archean life arose rapidly on Earth, indicated by their (disputed) geological record, suggesting that archaea may have arisen under

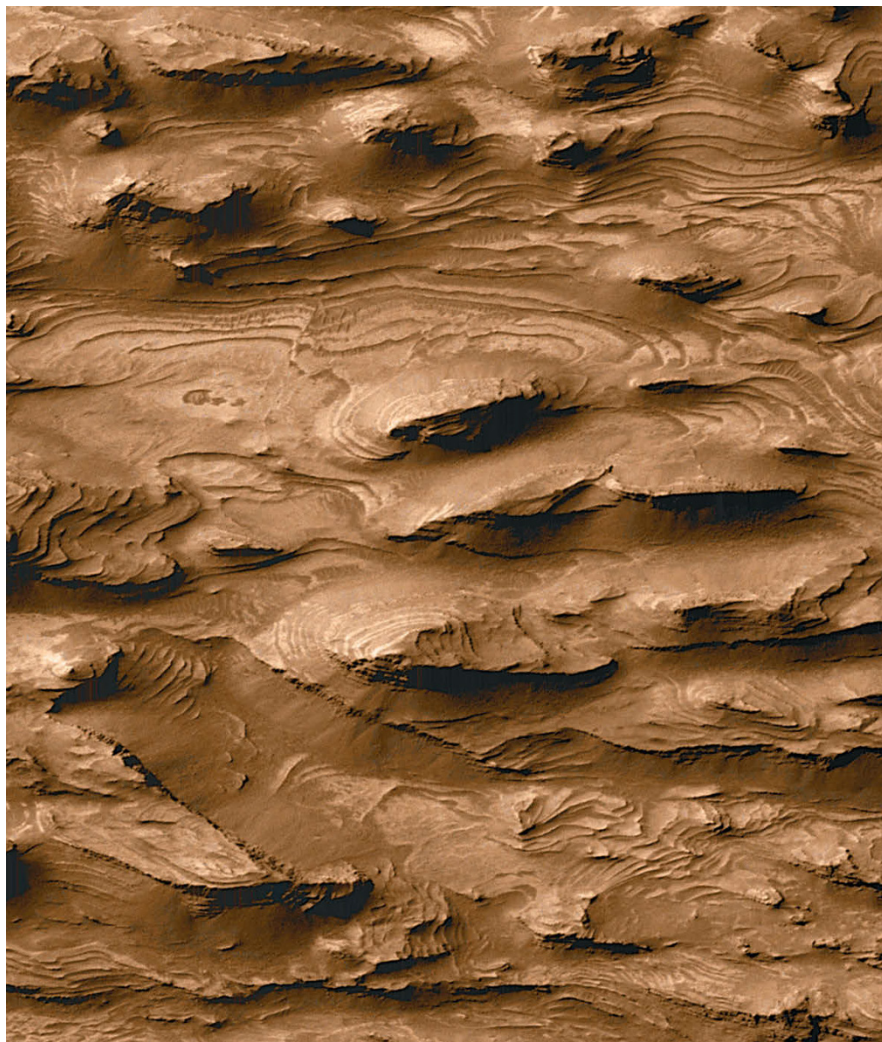


**Figure 2.9.** Layered sedimentary deposits on Mars [credit NASA].

similar conditions on Mars at this time. Assuming Earth-like evolution with similar starting ingredients and conditions, early surface pioneers of Mars may have resembled the cyanobacteria found in the 3.5 Gyr old record of Apex Chert on Earth which currently dominate in Antarctic deserts. Liquid water lakes could have persisted under protective ice cover for significant periods even as the climate gets progressively colder resembling the ice-covered lakes of the Antarctic Dry Valleys. These lakes remain liquid by geothermal energy input but are overlain by



3–5 m of ice (e.g., Lake Hoare). Hydrothermal systems may result from volcanic hot spots for several million years and cause the flow of mineral-rich fluids through rifts and faults though there is no evidence of shallow extant volcanic activity [91]. The most likely site for such is the Tharsis region which is the youngest volcanic region on Mars. It is plausible that Antarctic conditions are representative—endolithic organisms exhibit metabolic activity with little water and there may exist similar or dormant reservoirs of organisms on Mars. Photosynthetic organisms in polar soil biofilms, in the stromatolites of the beds of ice-covered lakes, and in the endolithic communities of translucent sandstone of the Trans-Antarctic Mountains represent potentially diverse habitats. Some microbial compounds (e.g., hopanoids, porphyrins, and isoprenoids) are recalcitrant and are found in the fossil record up to 2.5 Gyr ago. These represent potential analogs to possible extinct Martian biota. There is little doubt that Martian lacustrine deposits represent high-priority targets for astrobiological exploration. Although there exists little evidence of Noachian lacustrine activity due to erosion, lacustrine activity indicated by paleolake deltas was maximum during the Upper Hesperian period (2.5–2.1 Gyr ago) which decreased during the Amazonian epoch [92]. There are deepwater paleolakes indicating wave-cut terraces near their rims and flat floors with deltas at the mouths of inflowing channels and rarer dry palaeolakes which have high albedo [93]. The former are likely to contain increasingly fine sediment towards the central regions of the lake—gravel, sand, silt, and clays. As the water supply evaporated, evaporates were precipitated from the briny solutions. Carbonates are likely to be deposited centrally from both chemical and biological processes. Dry lakes may experience only periodic flooding and comprise evaporite salts such as carbonates, sulfates, etc. precipitated during the evaporation of water. Evaporites provide a signature for the former presence of water under hot conditions. Large evaporate deposits on Mars have yet to be identified but evaporitic conditions are expected to have existed on Mars (e.g., Wegener crater at 64.3°S, 4°W). Indeed, remnants of life may have been preserved within saline brine pockets within permafrost during Mars' dehydration and cooling which subsequently dried to form evaporites—predominantly halite (NaCl), gypsum ( $\text{CaSO}_4 \cdot 2\text{H}_2\text{O}$ ) and anhydrite ( $\text{CaSO}_4$ ) on Earth. It is conceivable that viable archeal and bacterial halophiles may survive in the frozen state, though the duration of such survival has yet to be established [94]. Caves would be a primary site for investigation as they represent the sites of underground water channel conduits. One of the most promising future sites for exploration is the Elysium Planitia adjacent to the 160 km diameter Gusev crater which terminates in a large branch of the Ma'adim Vallis valley network. They indicate evidence of a subsurface lake of ice beneath the soil.

The problem of dust also afflicts the Martian surface though its behavior is different. Mars is an eolian environment with seasonal dust storms and ever-present dust devils. The problem of dust sealing of mechanisms on the Moon and Mars are similar. On Sojourner, dust sealing was accomplished through the use of Delrin balls as output bearings in anodized Al races without lubrication at movable joints which provided tolerance to dust contamination.

<http://www.springer.com/978-3-642-03258-5>

Planetary Rovers

Robotic Exploration of the Solar System

Ellery, A.

2016, XXIX, 702 p. 155 illus., 119 illus. in color.,

Hardcover

ISBN: 978-3-642-03258-5